

RIS-aided secure communications over Fisher-Snedecor \mathcal{F} Fading Channels

Farshad Rostami Ghadi and Wei-Ping Zhu

Abstract—In this paper, we investigate the performance of physical layer security (PLS) over reconfigurable intelligent surfaces (RIS)-aided wireless communication systems, where all fading channels are modeled with Fisher-Snedecor \mathcal{F} distribution. Specifically, we consider a RIS with N reflecting elements between the transmitter and the legitimate receiver to develop a smart environment and also meliorate secure communications. In this regard, we derive the closed-form expressions for the secrecy outage probability (SOP) and average secrecy capacity (ASC). Monte-Carlo (MC) simulation results are provided throughout to validate the correctness of the developed analytical results, showing that considering RIS in wireless communication systems has constructive effects on the secrecy performance.

Index Terms—Physical layer security, reconfigurable intelligent surfaces, Fisher-Snedecor \mathcal{F} fading channels, secrecy outage probability, average secrecy capacity.

I. INTRODUCTION

Reconfigurable intelligent surfaces (RISs) have been recently offered as a cost-effective technique to enhance reliability and improve the performance of future wireless communications [1]. Specifically, RISs are artificial surfaces that are made of electromagnetic material and have a large number of passive reflecting elements, which can intelligently control the wireless propagation environment and ameliorate the received signal quality. On the other hand, the explosive growth in using wireless smart devices and also the broadcast nature of wireless channels have made momentous challenges for security and privacy in designing future wireless networks such as sixth-generation (6G) technology. One flexible approach to protect information from unauthorized access and guarantee secure communication is physical layer security (PLS). Given that PLS, which is widely referred to as the classic wiretap channel [2], leverages the physical characteristics of the propagation environment, accurate modeling of the statistical characteristics of fading channel coefficients is very important. To this end, the Fisher-Snedecor \mathcal{F} distribution has been recently introduced in [3] to correctly model the combined effects of shadowing and multipath fading in wireless device-to-device (D2D) communications. The main advantage of Fisher-Snedecor \mathcal{F} distribution is to provide a better tail matching of the empirical cumulative density function (CDF) for composite fading compared with the Generalized- \mathcal{K} model. Therefore, since the empirical CDF tail represents deep fading, the Fisher-Snedecor \mathcal{F} distribution is one of the best practical

scheme for modeling fading channels in wireless networks. In addition, the probability density function (PDF) of Fisher-Snedecor \mathcal{F} only consists of elementary functions with respect to the random variable (RV), thereby it can provide a more tractable analysis than the Generalized- \mathcal{K} model.

In recent years, intense research activities have been carried out on the role of RIS in PLS from various aspects [4]–[6], however, there are limited works in the context of RIS-aided secure communications over different fading channels [7]–[10]. For instance, the secrecy performance of RIS-aided communications under Rayleigh fading channels was investigated in [7], assuming the eavesdropper also can receive signals from the RIS. By deriving the closed-form expression for the secrecy outage probability (SOP), the authors showed that the system with the RIS and without the RIS-eavesdropper link has the best secrecy performance, which means that the secrecy performance becomes worse when the eavesdropper also utilizes the advantage of the RIS. In [8], assuming there is no direct link between transmitter and legitimate receiver, the authors studied secure vehicle-to-vehicle (V2V) communications under Rayleigh fading and derived a closed-form expression for the SOP in terms of the bivariate Fox H-function. Furthermore, the authors in [9], [10] studied RIS-aided secure communication systems under Nakagami- m and Fisher-Snedecore \mathcal{F} fading channels, respectively. The authors in [10] derived the SOP and the average secrecy capacity (ASC) under Fisher-Snedecore \mathcal{F} fading channels under a specific scenario, where only the transmitter uses a RIS-based access point (AP) for transmission and there is no RIS node between the transmitter and legitimate receiver.

Motivated by the potential of RIS and PLS technologies in performance improvement of future wireless communication systems and the significant role of Fisher-Snedecor \mathcal{F} distribution in accurate modeling and characterization of the simultaneous occurrence of multipath fading and shadowing, in this paper, we considered a RIS-aided secure communication system over Fisher-Snedecor \mathcal{F} fading channels. Specifically, in order to evaluate the effect of RIS deployment as well as fading severity on the PLS performance, we first provide analytical expressions for the PDF and the CDF of signal-to-noise ratios (SNRs), and then we derived the SOP and the ASC in closed-form expressions. Eventually, Monte-Carlo (MC) simulation results validate the accuracy of the analytical results. To the best of the authors' knowledge, our analytical expressions are novel in the context of RIS-aided secure communication systems and can be beneficial in practical applications due to their tightness and simplicity.

Notations: $\mathbb{E}(\cdot)$ and $\text{Var}(\cdot)$ are the expectation and variance operators respectively, $\Gamma(\cdot)$ and $\gamma(\cdot, \cdot)$ are the complete and

Manuscript received August xx, 2022; revised XXX.

F.R. Ghadi is with Departamento de Ingenieria de Comunicaciones, Universidad de Malaga - Campus de Excelencia Internacional Andalucía Tech., Malaga 29071, Spain, and W.P. Zhu is with Department of Electrical and Computer Engineering, Concordia University, Montreal, QC H3G 1M8, Canada. (e-mail: farshad@ic.uma.es, weiping@ece.concordia.ca).

Digital Object Identifier 10.1109/XXX.2021.XXXXXXX

incomplete Gamma functions respectively [11, Eqs. (8.31) and (8.35)], $B(\cdot, \cdot)$ is the Beta function [11, Eq. (8.38)], $G_{p,q}^{m,n}(\cdot)$ and $G_{p,q;p_1,q_1,p_2,q_2}^{m,n}(\cdot)$ are the univariate and bivariate Meijer's G-functions respectively [11, Eq. (9.3)], [12], and $H_{p,q;u,v,e,f}^{m,n;s,t;i,j}(\cdot)$ is the extended generalized bivariate Fox H-function [13, Eq. (2.56)].

II. SYSTEM MODEL

A. Channel Model

We consider a secure wireless communication scenario as shown in Fig. 1, where a legitimate transmitter (Alice) wants to send a confidential message to a legitimate receiver (Bob) aided by a RIS with N reflecting elements, while a passive eavesdropper (Eve) attempts to decode the message sent by Alice. For simplicity, we assume that all nodes are only equipped with single antennas. It is also assumed that the channel state information (CSI) of the legitimate receiver is known to Alice, and thus the RIS can efficiently implement phase shifting in order to maximize the received SNR at Bob. The received signal reflected by the RIS at Bob and the received signal at Eve can be respectively expressed as:

$$Y_B = \mathbf{g}_{AR}^T \Phi \mathbf{h}_{RB} X + Z_B, \quad (1)$$

$$Y_E = h_{AE} X + Z_E, \quad (2)$$

where X is the transmitted signal, Z_B and Z_E denote the additive white Gaussian noise (AWGN) with zero mean and variances σ_B^2 and σ_E^2 at Bob and Eve respectively, h_E is the fading coefficient from Alice to Eve, and Φ is the adjustable phase induced by the n th reflecting meta-surface of the RIS which defined as $\Phi = \text{diag}([e^{j\phi_1}, e^{j\phi_2}, \dots, e^{j\phi_N}])$. The vector \mathbf{g}_{AR}^T contains the channel gains from Alice to each element of the RIS and vector \mathbf{h}_{RB} includes the channel gains from each element of RIS to Bob, which are given by $\mathbf{g}_{AR} = d_{AR}^{-\alpha} [g_1 e^{-j\psi_1}, g_2 e^{-j\psi_2}, \dots, g_M e^{-j\psi_N}]^T$ and $\mathbf{h}_{RB} = d_{RB}^{-\alpha} [h_1 e^{-j\theta_1}, h_2 e^{-j\theta_2}, \dots, h_M e^{-j\theta_N}]^T$, where d_{AR} denotes the distance between Alice and the RIS, d_{RB} is the distance between the RIS and Bob, and α defines the path-loss exponent. The terms g_n and h_n , $n \in \{1, 2, \dots, N\}$ are the amplitudes of the corresponding channel gains, and $e^{-j\psi_n}$ and $e^{-j\theta_n}$ denote the phase of the respective links. We assume that all fading channel coefficients are modeled by the independent Fisher-Snedecor \mathcal{F} distribution with fading parameters (m_{s_k}, m_k) so that m_{s_k} and m_k represent the amount of shadowing of the root-mean-square (rms) signal power and the fading severity parameter, respectively.

B. SNR Distribution

1) *The main link:* From (1), the instantaneous SNR at Bob can be expressed as:

$$\gamma_B = \frac{P \left| \sum_{n=1}^N g_n h_n e^{j(\phi_n - \psi_n - \theta_n)} \right|^2}{\sigma_B^2 d_{AR}^\alpha d_{RB}^\alpha}, \quad (3)$$

$$\stackrel{(a)}{=} \frac{P \left| \sum_{n=1}^N g_n h_n \right|^2}{\sigma_B^2 d_{AR}^\alpha d_{RB}^\alpha} = \bar{\gamma}_B W, \quad (4)$$

where $\bar{\gamma}_B$ is the average SNR at Bob and (a) is obtained by considering perfect knowledge of the CSI at RIS, which

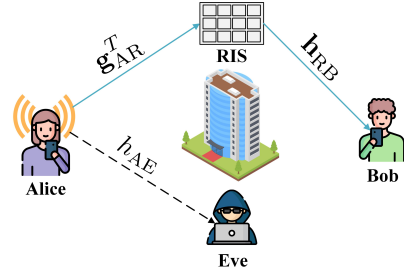


Fig. 1. System model depicting the RIS-aided secure communications.

provides the ideal phase shifting (i.e., $\phi_n = \psi_n + \theta_n$) for maximizing the SNR at Bob [7]. In the following theorem, we present the distributions of γ_B , assuming that g_n and h_n follow independent Fisher-Snedecor \mathcal{F} distribution.

Theorem 1. Assuming all channels follow Fisher-Snedecor \mathcal{F} fading model, the PDF and the CDF of γ_B are respectively determined as:

$$f_{\gamma_B}(\gamma_B) = \frac{\gamma_B^{(a-1)/2}}{2\bar{\gamma}_B^{(a+1)/2} b^{a+1} \Gamma(a+1)} e^{-\frac{\sqrt{\gamma_B}}{b\sqrt{\bar{\gamma}_B}}}, \quad (5)$$

$$F_{\gamma_B}(\gamma_B) = \frac{\gamma \left(a+1, \frac{\sqrt{\gamma_B}}{b\sqrt{\bar{\gamma}_B}} \right)}{\Gamma(a+1)}, \quad (6)$$

where Ω_k for $k \in \{R, B\}$ is the mean power,

$$a = \frac{(N+1)B^2 - AC}{AC - B^2}, \quad b = \frac{D(AC - B^2)}{BC},$$

$$A = B(m_B + 1, m_{s_B} - 1) B(m_R + 1, m_{s_R} - 1),$$

$$B = B\left(m_B + \frac{1}{2}, m_{s_B} - \frac{1}{2}\right) B\left(m_R + \frac{1}{2}, m_{s_R} - \frac{1}{2}\right),$$

$$C = B(m_B, m_{s_B}) B(m_R, m_{s_R}), \text{ and}$$

$$D = \left(\frac{m_B m_R}{(m_{s_B} - 1)(m_{s_R} - 1) \Omega_B \Omega_R} \right)^{-\frac{1}{2}}.$$

Proof. The details of proof are in Appendix A. \square

2) *The eavesdropping link:* From (2), the instantaneous SNR at Eve is given by $\gamma_E = \frac{P|h_E|^2}{\sigma_E^2 d_{AE}^\alpha} = \bar{\gamma}_E g_E$, where d_{AE} denotes the distance between Alice and Eve, $g_E = |h_E|^2$ represents the instantaneous channel power gain with unit mean, and $\bar{\gamma}_E$ is the average SNR at Eve. The PDF and the CDF of the instantaneous SNR γ_E can be defined in terms of Meijer's as [14]:

$$f_{\gamma_E}(\gamma_E) = \mathcal{E}_E G_{1,1}^{1,1} \left(\lambda_E \gamma_E \left| \begin{matrix} -m_{s_E} \\ m_E - 1 \end{matrix} \right. \right), \quad (7)$$

$$F_{\gamma_E}(\gamma_E) = \mathcal{G}_E G_{2,2}^{1,2} \left(\lambda_E \gamma_E \left| \begin{matrix} (1 - m_{s_E}, 1) \\ (m_E, 0) \end{matrix} \right. \right), \quad (8)$$

where $\lambda_E = \frac{m_E}{\bar{\gamma}_E m_{s_E}}$, $\mathcal{E}_E = \frac{\lambda_E}{\Gamma(m_E) \Gamma(m_{s_E})}$, and $\mathcal{G}_E = \frac{\Gamma(m_E + 1)}{m_E \Gamma(m_E) \Gamma(m_E + m_{s_E}) B(m_E, m_{s_E})}$.

III. SECRECY PERFORMANCE ANALYSIS

In this section, we derive closed-form expressions of the SOP and the ASC for the considered system model.

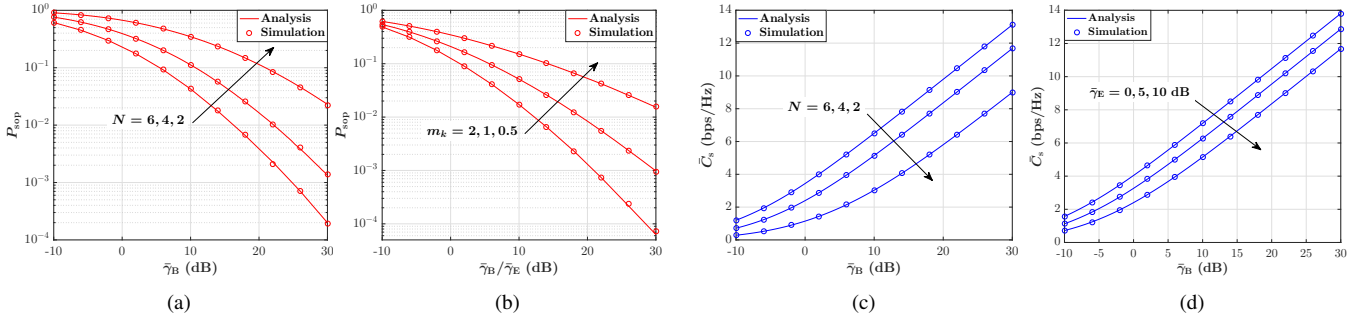


Fig. 2. (a) SOP versus $\bar{\gamma}_B$ for selected values of N , when $\bar{\gamma}_E = 10\text{dB}$, $R_s = 1$ and $(m_{s_k}, m_k) = (3, 2)$, $k \in \{B, R, E\}$; (b) SOP versus $\bar{\gamma}_B/\bar{\gamma}_E$ for selected values of m_k , when $N = 4$, $m_{s_k} = 3$, and $R_s = 1$; (c) ASC versus $\bar{\gamma}_B$ for selected values of N , when $\bar{\gamma}_E = 10\text{dB}$, $R_s = 1$ and $(m_{s_k}, m_k) = (3, 2)$; (d) SOP versus $\bar{\gamma}_B$ for selected values of $\bar{\gamma}_E$, when $N = 4$, $R_s = 1$, and $(m_{s_k}, m_k) = (3, 2)$.

A. SOP analysis

The SOP is an information-theoretical metric to evaluate the performance of physical layer security, which is defined as the probability that the instantaneous secrecy capacity C_s is less than a target secrecy rate $R_s > 0$, $P_{\text{sop}} = \Pr(C_s \leq R_s)$, where C_s for the considered system model can be defined as:

$$C_s(\gamma_B, \gamma_E) = \max\{\ln(1 + \gamma_B) - \ln(1 + \gamma_E), 0\}. \quad (9)$$

Now, by inserting (9) into SOP definition, P_{sop} for the considered model is mathematically expressed as:

$$P_{\text{sop}} = \Pr\left(\ln\left(\frac{1 + \gamma_B}{1 + \gamma_E}\right) \leq R_s\right), \quad (10)$$

$$= \int_0^\infty F_{\gamma_B}(\gamma_t) f_{\gamma_E}(\gamma_E) d\gamma_E, \quad (11)$$

where $\gamma_t = (1 + \gamma_E)e^{R_s} - 1 = \gamma_E R_t + R_t - 1 = \gamma_E R_t + \bar{R}_t$.

Theorem 2. *The SOP for the considered RIS-aided secure communication system under Fisher-Snedecor \mathcal{F} fading channels is given by*

$$P_{\text{sop}} = H_{1,0:1,2:1,2}^{0,1:1,1:2,1} \left(\frac{b\sqrt{\bar{\gamma}_B}}{\sqrt{\bar{R}_t}}, \frac{R_t}{\bar{R}_t \lambda_E} \left| \begin{array}{c} \mathcal{I}_1 \\ - \end{array} \right| \begin{array}{c} \mathcal{I}_2 \\ \mathcal{J}_2 \end{array} \left| \begin{array}{c} \mathcal{I}_3 \\ \mathcal{J}_3 \end{array} \right. \right), \quad (12)$$

where $\mathcal{I}_1 = (2; \frac{1}{2}, 1)$, $\mathcal{I}_2 = (-a, 1)$, $\mathcal{I}_3 = (2 - m_E, 1)$, $\mathcal{J}_2 = (0, 1)$, and $\mathcal{J}_3 = (1, 1), (1 + m_{s_E}, 1)$.

Proof. The details of proof are in Appendix B. \square

B. ASC analysis

Here, we define the ASC for the system model under consideration, as:

$$\bar{C}_s \triangleq \int_0^\infty \int_0^\infty C_s(\gamma_B, \gamma_E) f_{\gamma_B}(\gamma_B) f_{\gamma_E}(\gamma_E) d\gamma_B d\gamma_E. \quad (13)$$

Theorem 3. *The ASC for the considered RIS-aided secure communication system under Fisher-Snedecor \mathcal{F} fading channels is given by*

$$\begin{aligned} \bar{C}_s &= \mathcal{H} H_{1,0:2,2:1,2}^{0,2:1,1:2,2,1} \left(\frac{b\sqrt{\bar{\gamma}_B}}{\sqrt{\bar{R}_t}}, \frac{R_t}{\bar{R}_t \lambda_E} \left| \begin{array}{c} \mathcal{U}_1 \\ - \end{array} \right| \begin{array}{c} \mathcal{U}_2 \\ \mathcal{V}_2 \end{array} \left| \begin{array}{c} \mathcal{U}_3 \\ \mathcal{V}_3 \end{array} \right. \right) \\ &+ \mathcal{O} G_{1,1:2,1:2,2}^{1,1:1,1:1,2} \left(\frac{1}{b^2 \bar{\gamma}_B \bar{\gamma}_E}, \frac{1}{\lambda_E} \left| \begin{array}{c} m_E \\ m_{s_E} \end{array} \right| \begin{array}{c} 1 \\ (a+1, 0) \end{array} \left| \begin{array}{c} (1, 1) \\ (1, 0) \end{array} \right. \right) \\ &- \frac{\mathcal{O}}{2} G_{3,2}^{2,3} \left(\frac{1}{\lambda_E} \left| \begin{array}{c} (1, 1, 1 - m_E) \\ (1, m_{s_E}, 0) \end{array} \right. \right), \quad (14) \end{aligned}$$

where $\mathcal{H} = \frac{\mathcal{G}_E}{b^{a+1} \Gamma(a+1) \ln 2 \sqrt{2\pi}}$, $\mathcal{O} = \frac{2\mathcal{E}_E}{\lambda_E \ln 2}$, $\mathcal{U}_1 = (\frac{-a}{2}; 1, 1)$, $(\frac{1-a}{2}; 1, 1)$, $\mathcal{U}_2 = (1 - m_{s_E}, 1), (1, 1)$, $\mathcal{U}_3 = (1, 1), (1, 1)$, $\mathcal{V}_2 = (m_E, 1), (0, 1)$, and $\mathcal{V}_3 = (1, 1), (1, 1)$.

Proof. The details of proof are in Appendix C. \square

IV. NUMERICAL RESULTS

In this section, we evaluate the theoretical expressions previously derived, which are double-checked in all instances with Monte-Carlo (MC) simulations.

Fig. 2(c) illustrates the behavior of the SOP in terms of $\bar{\gamma}_B$ for the selected value of N under Fisher-Snedecor \mathcal{F} fading channels. It can be seen as the number of RIS reflecting elements increases the SOP performance improves even if the main channel's condition is worse than the eavesdropper's channel (i.e., $\bar{\gamma}_B \leq \bar{\gamma}_E$). The reason is that exploiting the RIS can provide a channel with higher quality and also enhance the received SNR when phase processing is utilized. Fig. 2(b) shows the SOP performance in terms of $\bar{\gamma}_B/\bar{\gamma}_E$ for different values of fading parameters m_k , $k \in \{R, B, E\}$ under RIS deployment between Alice and Bob. We can see that as the fading is less severe (i.e., as m_k increases) the SOP performance improves, meaning that system performance ameliorates (degrades) in environments that exhibit light (heavy) fading characteristics. Figs. 2(c) and 2(d) represent the ASC performance based on the variation of $\bar{\gamma}_B$ for selected values of N and $\bar{\gamma}_E$, respectively. As shown in Fig. 2(c), a relatively small increase in the number of RIS reflecting elements has a constructive impact on the ASC performance, regardless of the main and eavesdropper channels condition. Fig. 2(d) shows that under RIS deployment and Fisher-Snedecor \mathcal{F} fading channels, the ASC performance improves as $\bar{\gamma}_B$ grows. Moreover, we can see that the ASC can still be achieved even if $\bar{\gamma}_B \leq \bar{\gamma}_E$.

V. CONCLUSION

In this paper, we studied the secrecy performance of a RIS-aided wireless communication system under Fisher-Snedecor \mathcal{F} fading channels. In particular, we first presented the analytical expressions for the PDF and the CDF of corresponding SNRs, and then we derived the closed-form expressions of the SOP and the ASC. The simulation results validated the accuracy of analytical results and showed that the considering RIS between the transmitter and the legitimate receiver has constructive effects on system performance in terms of the SOP and ASC.

APPENDIX A
PROOF OF THEOREM 1

Let $W_n = G_n H_n$ be the product of two independent Fisher-Snedecor \mathcal{F} RVs. Then, the PDF of W_n is defined as [15]:

$$f_{W_n}(w_n) = \frac{2w_n^{-1}}{\Gamma(m_R)\Gamma(m_{s_R})\Gamma(m_B)\Gamma(m_{s_B})} \times G_{2,2}^{2,2} \left(w_n^2 \frac{m_R m_B}{(m_{s_R}-1)(m_{s_B}-1)\omega_2 \omega_1} \middle| \begin{matrix} 1 - m_{s_R}, 1 - m_{s_B} \\ m_R, m_B \end{matrix} \right). \quad (15)$$

The mean and variance of W_i are respectively given by [15]

$$\mathbb{E}(W_n) = \frac{B(m_B + \frac{1}{2}, m_{s_B} - \frac{1}{2}) B(m_R + \frac{1}{2}, m_{s_R} - \frac{1}{2})}{B(m_B, m_{s_B}) B(m_R, m_{s_R})} \times \left(\frac{m_B m_R}{(m_{s_B} - 1)(m_{s_R} - 1)\Omega_B \Omega_R} \right)^{-\frac{1}{2}}, \quad (16)$$

$$\text{Var}(W_n) = \frac{(m_{s_B} - 1)(m_{s_R} - 1)\Omega_B \Omega_R}{m_B m_R B(m_B, m_{s_B}) B(m_R, m_{s_R})} \times \left[\frac{B(m_B + \frac{1}{2}, m_{s_B} - \frac{1}{2})^2 B(m_R + \frac{1}{2}, m_{s_R} - \frac{1}{2})^2}{B(m_B, m_{s_B}) B(m_R, m_{s_R})} - B(m_B + 1, m_{s_B} - 1) B(m_R + 1, m_{s_R} - 1) \right]. \quad (17)$$

Now, by exploiting the first term of a Laguerre expansion [16, Sec. 2.2.2], the PDF of $W = \sum_{n=1}^N W_n$ can be accurately determined as:

$$f_W(w) = \frac{w^a}{b^{a+1}\Gamma(a+1)} e^{-\frac{w}{b}}, \quad (18)$$

where $a = \frac{N\mathbb{E}(W_n)^2}{\text{Var}(W_n)} - 1$ and $b = \frac{\text{Var}(W_n)}{\mathbb{E}(W_n)}$. Eventually, by performing the RV transformation $f_{\gamma_B}(\gamma_B) = \frac{1}{2\sqrt{\gamma_B}} f_W\left(\sqrt{\frac{\gamma_B}{\gamma_B}}\right)$, the PDF of γ_B is obtained as (5). Besides, by using definition $F_{\gamma_B}(\gamma_B) = \int_0^\gamma f_{\gamma_B}(x) dx$, and then computing the corresponding integral, the CDF of γ_B is also achieved as (6).

APPENDIX B
PROOF OF THEOREM 2

By exploiting the Parseval relation for Mellin transform [17, Eq. (8.3.23)], (11) can be rewritten as follows:

$$P_{\text{sop}} = \frac{1}{2\pi j} \int_{\mathcal{L}_1} \mathcal{M}[F_{\gamma_B}(\gamma_t), 1-s] \mathcal{M}[f_{\gamma_E}(\gamma_E), s] ds, \quad (19)$$

where \mathcal{L}_1 is the integration path from $\nu - j\infty$ to $\nu + j\infty$ for a constant value of ν [3]. Then, by using the definition of Meijer's G-function, $\mathcal{M}[F_{\gamma_B}(\gamma_t), 1-s]$ can be obtained as:

$$\mathcal{M}[F_{\gamma_B}(\gamma_t), 1-s] = \int_0^\infty \gamma_E^{-s} F_{\gamma_B}(\gamma_t) d\gamma_E, \quad (20)$$

$$\stackrel{(a)}{=} \int_0^\infty \gamma_E^{-s} G_{1,2}^{1,1} \left(\frac{\sqrt{\gamma_t}}{b\sqrt{\gamma_B}} \middle| \begin{matrix} 1 \\ a+1, 0 \end{matrix} \right) d\gamma_E, \quad (21)$$

$$\stackrel{(b)}{=} \frac{1}{2\pi j} \int_{\mathcal{L}_2} \int_0^\infty \gamma_E^{-s} \frac{\Gamma(a+1+\zeta)\Gamma(-\zeta)}{\Gamma(1-\zeta)} \left(\frac{\sqrt{\gamma_t}}{b\sqrt{\gamma_B}} \right)^{-\zeta} d\gamma_E d\zeta, \quad (22)$$

where (a) is obtained by converting the incomplete Gamma function in (6) into Meijer's G-function, and (b) is achieved by exploiting the definition of Meijer's G-function and interchanging the integrals order. With the help of [11, Eq. (3.194.3)], the inner integral in (22) can be computed as:

$$\int_0^\infty \gamma_E^{-s} \gamma_t^{-\zeta/2} d\gamma_E \stackrel{(c)}{=} \int_0^\infty \frac{\gamma_E^{-s}}{(\gamma_E R_t + \bar{R}_t)^{\zeta/2}} d\gamma_E, \quad (23)$$

$$\stackrel{(d)}{=} \bar{R}_t^{-\zeta/2} \left(\frac{R_t}{\bar{R}_t} \right)^{s-1} B\left(1-s, \frac{\zeta}{2} + s - 1\right), \quad (24)$$

$$\stackrel{(e)}{=} \bar{R}_t^{-\zeta/2} \left(\frac{R_t}{\bar{R}_t} \right)^{s-1} \frac{\Gamma(1-s)\Gamma\left(\frac{\zeta}{2} + s - 1\right)}{\Gamma\left(\frac{\zeta}{2}\right)}, \quad (25)$$

where (c) is obtained representing $\gamma_t = \gamma_E R_t + \bar{R}_t$, (d) is derived from [11, Eq. (3.194.3)], and (e) is obtained by utilizing the property of beta function where $B(a_1, b_1) = \frac{\Gamma(a_1)\Gamma(b_1)}{\Gamma(a_1+b_1)}$. Now, by inserting (25) into (22), we have:

$$\mathcal{M}[F_{\gamma_B}(\gamma_t), 1-s] = \frac{\Gamma(1-s)}{2\pi j} \left(\frac{R_t}{\bar{R}_t} \right)^{s-1} \times \int_{\mathcal{L}_2} \frac{\Gamma(a+1+\zeta)\Gamma(-\zeta)\Gamma\left(\frac{\zeta}{2} + s - 1\right)}{\Gamma\left(\frac{\zeta}{2}\right)\Gamma(1-\zeta)} \left(\frac{\sqrt{R_t}}{b\sqrt{\gamma_B}} \right)^{-\zeta} d\zeta, \quad (26)$$

where \mathcal{L}_2 is a specific counter. Next, with the aid of [13, Eq. (2.9)], the Mellin transform $\mathcal{M}[f_{\gamma_E}(\gamma_E), s]$ is given by

$$\mathcal{M}[f_{\gamma_E}(\gamma_E), s] = \mathcal{E}_E \int_0^\infty \gamma_E^{s-1} G_{1,1}^{1,1} \left(\lambda_E \gamma_E \middle| \begin{matrix} -m_{s_E} \\ m_E - 1 \end{matrix} \right) d\gamma_E, \quad (27)$$

$$= \mathcal{E}_E \frac{\Gamma(m_E - 1 + s)\Gamma(1 + m_{s_E} - s)}{\lambda_E^s}. \quad (28)$$

Then, by substituting (26) and (28) into (19), P_{sop} can be written as:

$$P_{\text{sop}} = \frac{\mathcal{E}_E \bar{R}_t}{R_t} \left(\frac{1}{2\pi j} \right)^2 \int_{\mathcal{L}_1} \int_{\mathcal{L}_2} \left(\frac{b\sqrt{\gamma_B}}{\sqrt{R_t}} \right)^\zeta \left(\frac{R_t}{\bar{R}_t \lambda_E} \right)^s \times \Gamma\left(\frac{\zeta}{2} + s - 1\right) \frac{\Gamma(a+1+\zeta)\Gamma(-\zeta)}{\Gamma\left(\frac{\zeta}{2}\right)\Gamma(1-\zeta)} \Gamma(1-s) \times \Gamma(m_E - 1 + s)\Gamma(1 + m_{s_E} - s) d\zeta ds. \quad (29)$$

Eventually, by exploiting the representation of bivariate Fox H-function in terms of double contour integral [13, Eq. (2.56)], the proof is completed.

APPENDIX C
PROOF OF THEOREM 3

By inserting (9) into (13), \bar{C}_s can be expressed as:

$$\bar{C}_s = \int_0^\infty \log_2(1 + \gamma_B) f_{\gamma_B}(\gamma_B) F_{\gamma_E}(\gamma_B) d\gamma_B + \int_0^\infty \log_2(1 + \gamma_E) f_{\gamma_E}(\gamma_E) F_{\gamma_B}(\gamma_E) d\gamma_E \quad (30)$$

$$- \int_0^\infty \log_2(1 + \gamma_E) f_E(\gamma_E) d\gamma_E = I_1 + I_2 - I_3. \quad (31)$$

Next, by substituting the marginal distributions from (5) and (6) into (31), and re-expressing the logarithm function and

the incomplete Gamma function in terms of the Meijer's G-function [18], I_1 can be determined as:

$$\begin{aligned}
I_1 &= \frac{\mathcal{G}_E}{2\bar{\gamma}_B^{(a+1)/2} b^{a+1} \Gamma(a+1) \ln 2} \int_0^\infty G_{2,2}^{1,2} \left(\gamma_B \left| \begin{matrix} (1,1) \\ (1,0) \end{matrix} \right. \right) \\
&\times G_{2,2}^{1,2} \left(\lambda_E \gamma_B \left| \begin{matrix} (1-m_{s_E}, 1) \\ (m_E, 0) \end{matrix} \right. \right) \gamma_B^{(a-1)/2} e^{-\frac{\sqrt{\gamma_B}}{b\sqrt{\gamma_B}}} d\gamma_B, \quad (32) \\
&\stackrel{(f)}{=} \frac{\mathcal{G}_E}{2\bar{\gamma}_B^{(a+1)/2} b^{a+1} \Gamma(a+1) \ln 2} \frac{1}{2\pi j} \int_{\mathcal{L}} \frac{\Gamma(1-s)\Gamma(s)\Gamma(s)}{\Gamma(1+s)} \\
&\times \underbrace{\int_0^\infty \gamma_B^{\frac{a-1}{2}+s} e^{-\frac{\sqrt{\gamma_B}}{b\sqrt{\gamma_B}}} G_{2,2}^{1,2} \left(\lambda_E \gamma_B \left| \begin{matrix} (1-m_{s_E}, 1) \\ (m_E, 0) \end{matrix} \right. \right) d\gamma_B ds,}_{J} \quad (33)
\end{aligned}$$

where (f) is obtained by using the definition Meijer's function. Then, with the help of [18, Eq. (2.24.3.1)], the inner integral J can be computed as:

$$\begin{aligned}
J &= \frac{2^{\frac{a+2s}{2}+1}}{\sqrt{2\pi}} \left(\frac{1}{\sqrt{\gamma_B}} \right)^{-(1+a+2s)} \\
&\times G_{4,2}^{1,4} \left(4b^2 \bar{\gamma}_B \lambda_E \left| \begin{matrix} -s - \frac{a}{2}, -s - \frac{a-1}{2}, 1 - m_{s_E}, 1 \\ (m_E, 0) \end{matrix} \right. \right), \quad (34)
\end{aligned}$$

By plugging (34) into (33), we have:

$$\begin{aligned}
I_1 &= \left(\frac{1}{2\pi j} \right)^2 \frac{\Phi_E}{b^{a+1} \Gamma(a+1) \ln 2} \frac{2^{a/2}}{\sqrt{2\pi}} \int_{\mathcal{L}_1} \int_{\mathcal{L}_2} (2\bar{\gamma}_B)^s (4b^2 \bar{\gamma}_B \lambda_E)^\zeta \\
&\times \frac{\Gamma(1-s)\Gamma(s)\Gamma(s)\Gamma(m_E-\zeta)\Gamma(m_{s_E}+\zeta)\Gamma(\zeta)}{\Gamma(1+s)\Gamma(1+\zeta)} \\
&\times \Gamma\left(1+s+\frac{a}{2}+\zeta\right) \Gamma\left(\frac{1}{2}+s+\frac{a}{2}+\zeta\right) d\zeta ds. \quad (35)
\end{aligned}$$

Consequently, recognizing the definition of bivariate Fox H-function, I_1 is derived as:

$$I_1 = \mathcal{H} H_{1,0;2,2;1,2;2,1}^{0,2;1,2;2,1} \left(\frac{b\sqrt{\gamma_B}}{\sqrt{R_t}}, \frac{R_t}{R_t \lambda_E} \left| \begin{matrix} \mathcal{U}_1 \\ - \end{matrix} \right. \left| \begin{matrix} \mathcal{U}_2 \\ \mathcal{V}_2 \end{matrix} \right. \left| \begin{matrix} \mathcal{U}_3 \\ \mathcal{V}_3 \end{matrix} \right. \right), \quad (36)$$

where $\mathcal{H} = \frac{\mathcal{G}_E}{b^{a+1} \Gamma(a+1) \ln 2} \frac{2^{a/2}}{\sqrt{2\pi}}$, $\mathcal{U}_1 = \left(\frac{-a}{2}; 1, 1\right)$, $\left(\frac{1-a}{2}; 1, 1\right)$, $\mathcal{U}_2 = (1-m_{s_E}, 1), (1, 1)$, $\mathcal{U}_3 = (1, 1), (1, 1)$, $\mathcal{V}_2 = (m_E, 1), (0, 1)$, and $\mathcal{V}_3 = (1, 1), (1, 1)$.

Following the same methodology, I_2 can be derived as:

$$\begin{aligned}
I_2 &= \int_0^\infty \log_2(1+\gamma_E) f_{\gamma_E}(\gamma_E) F_{\gamma_B}(\gamma_E) d\gamma_E \quad (37) \\
&\stackrel{(g)}{=} \frac{\mathcal{E}_E}{2\pi j \ln 2} \int_{\mathcal{L}_1} \frac{\Gamma(a+1-s)\Gamma(s)}{\Gamma(1+s)} \frac{1}{b\sqrt{\gamma_B}} \int_0^\infty \gamma_E^{\frac{s}{2}} \\
&\times G_{2,2}^{1,2} \left(\gamma_E \left| \begin{matrix} (1,1) \\ (1,0) \end{matrix} \right. \right) G_{1,1}^{1,1} \left(\lambda_E \gamma_E \left| \begin{matrix} -m_{s_E} \\ m_E - 1 \end{matrix} \right. \right) d\gamma_E ds, \quad (38)
\end{aligned}$$

$$\begin{aligned}
&\stackrel{(h)}{=} \frac{2\mathcal{E}_E}{\lambda_E \ln 2} \left(\frac{1}{2\pi j} \right)^2 \int_{\mathcal{L}_1} \int_{\mathcal{L}_2} \left(\frac{1}{b^2 \bar{\gamma}_B \bar{\gamma}_E} \right)^\eta \left(\frac{1}{\gamma_E} \right)^\zeta \\
&\times \frac{\Gamma(a+1-\eta)\Gamma(\eta)\Gamma(1-\zeta)\Gamma(\zeta)^2}{\Gamma(1+\eta)\Gamma(1+\zeta)} \\
&\times \Gamma(m_E+\eta+\zeta)\Gamma(m_{s_E}-\eta-\zeta) d\zeta d\eta, \quad (39)
\end{aligned}$$

$$\stackrel{(i)}{=} \mathcal{O} G_{1,1;2,1;1,1;2,2}^{1,1;1,1;1,2} \left(\frac{1}{b^2 \bar{\gamma}_B \bar{\gamma}_E}, \frac{1}{\lambda_E} \left| \begin{matrix} m_E \\ m_{s_E} \end{matrix} \right. \left| \begin{matrix} 1 \\ (a+1, 0) \end{matrix} \right. \left| \begin{matrix} (1, 1) \\ (1, 0) \end{matrix} \right. \right), \quad (40)$$

where $\mathcal{O} = \frac{2\mathcal{E}_E}{\lambda_E \ln 2}$, step (g) is derived by exploiting Meijer's G function definition, (h) is obtained by computing the inner integral with the help of [18, Eq. (2.25.1.1)], and (i) is achieved by exploiting the definition of bivariate Fox H-function. Besides, with the help of [18, Eqs. (2.25.1.1) and (8.3.2.21)], I_3 is determined as $I_3 = \frac{\mathcal{O}}{2} G_{3,2}^{2,3} \left(\frac{1}{\lambda_E} \left| \begin{matrix} (1, 1, 1 - m_E) \\ (1, m_{s_E}, 0) \end{matrix} \right. \right)$.

REFERENCES

- [1] E. Basar, M. Di Renzo, J. De Rosny, M. Debbah, M.-S. Alouini, and R. Zhang, "Wireless communications through reconfigurable intelligent surfaces," *IEEE access*, vol. 7, pp. 116753–116773, 2019.
- [2] A. D. Wyner, "The wire-tap channel," *Bell system technical journal*, vol. 54, no. 8, pp. 1355–1387, 1975.
- [3] S. K. Yoo, S. L. Cotton, P. C. Sofotasios, M. Matthaiou, M. Valkama, and G. K. Karagiannidis, "The fisher–snedecor \mathcal{F} distribution: A simple and accurate composite fading model," *IEEE Commun. Lett.*, vol. 21, no. 7, pp. 1661–1664, 2017.
- [4] J. Zhang, H. Du, Q. Sun, B. Ai, and D. W. K. Ng, "Physical layer security enhancement with reconfigurable intelligent surface-aided networks," *IEEE Trans. Inf. Forensics Security*, vol. 16, pp. 3480–3495, 2021.
- [5] Z. Tang, T. Hou, Y. Liu, J. Zhang, and C. Zhong, "A novel design of ris for enhancing the physical layer security for ris-aided noma networks," *IEEE Wirel. Commun. Lett.*, vol. 10, no. 11, pp. 2398–2401, 2021.
- [6] I. Trigui, W. Ajib, and W.-P. Zhu, "Secrecy outage probability and average rate of ris-aided communications using quantized phases," *IEEE Commun. Lett.*, vol. 25, no. 6, pp. 1820–1824, 2021.
- [7] L. Yang, J. Yang, W. Xie, M. O. Hasna, T. Tsiftsis, and M. Di Renzo, "Secrecy performance analysis of ris-aided wireless communication systems," *IEEE Trans. Veh. Technol.*, vol. 69, no. 10, pp. 12296–12300, 2020.
- [8] Y. Ai, A. Felipe, L. Kong, M. Cheffena, S. Chatzinotas, and B. Ottersten, "Secure vehicular communications through reconfigurable intelligent surfaces," *IEEE Trans. Veh. Technol.*, vol. 70, no. 7, pp. 7272–7276, 2021.
- [9] A. K. Yadav, S. Yadav, A. Pandey, and A. Silva, "On the secrecy performance of ris-enabled wireless communications over nakagami-m fading channels," *ICT Express*, 2022.
- [10] A. Makarfi, K. Rabie, O. Badarneh, G. Naurzybayev, and R. Kharel, "Physical layer security in ris-assisted networks in fisher–snedecor composite fading," in *2020 12th Int. Symp. Commun. Syst. Netw. Digit. (CSNDSP)*. IEEE, 2020, pp. 1–6.
- [11] D. Zwillinger and A. Jeffrey, *Table of integrals, series, and products*. Elsevier, 2007.
- [12] S. Gupta, "Integrals involving products of g-function," *Proceedings of the National Academy of Sciences India Section A-Physical Sciences*, vol. 39, p. 193, 1969.
- [13] A. M. Mathai, R. K. Saxena, and H. J. Haubold, *The H-function: theory and applications*. Springer Science & Business Media, 2009.
- [14] F. R. Ghadi and W.-P. Zhu, "Performance analysis over correlated/independent fisher–snedecor f fading multiple access channels," *IEEE Trans. Veh. Technol.*, 2022.
- [15] O. S. Badarneh, P. C. Sofotasios, S. Muhaidat, S. L. Cotton, and D. B. Da Costa, "Product and ratio of product of fisher–snedecor \mathcal{F} variates and their applications to performance evaluations of wireless communication systems," *IEEE Access*, vol. 8, pp. 215267–215286, 2020.
- [16] S. Primak, V. Kontorovich, and V. Lyandres, *Stochastic methods and their applications to communications: stochastic differential equations approach*. John Wiley & Sons, 2005.
- [17] B. Davies, *Integral transforms and their applications*. Springer Science & Business Media, 2002, vol. 41.
- [18] A. Prudnikov, Y. A. Brychkov, and O. Marichev, "More special functions (integrals and series vol 3)," 1990.